

Spectroscopic insight into post-synthetic surface modification of porous glass beads as silica model system

Marianne Wenzel,^a Louisa Eckert,^b Kai Müller,^b Dmytro Solonenko,^c Christian Wiebeler,^{a,d} Dietrich R.T. Zahn,^c Dirk Enke^b and Jörg Matysik*^a

a. Institut für Analytische Chemie, Universität Leipzig, Linnéstr. 3, 04103 Leipzig, Germany

b. Institut für Technische Chemie, Universität Leipzig, Linnéstr. 3, 04103 Leipzig, Germany

c. Semiconductor Physics, Technische Universität Chemnitz, Reichenhainer Str. 70, 09107 Chemnitz, Germany

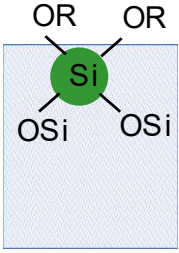
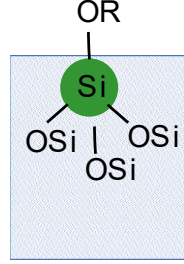
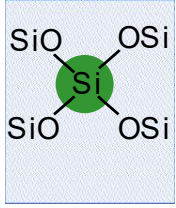
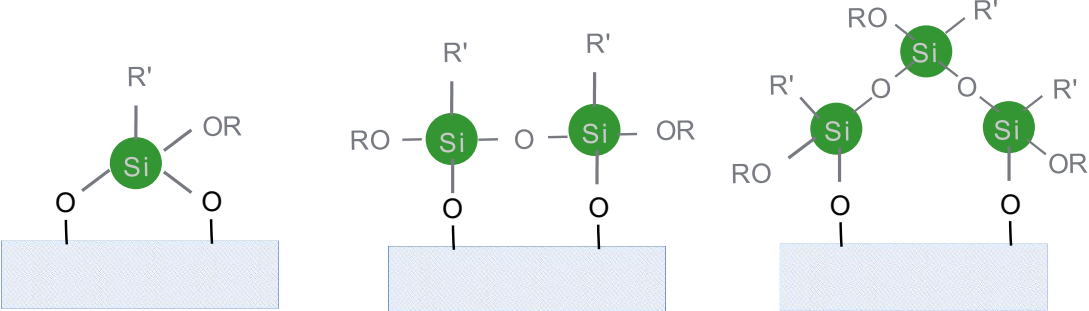
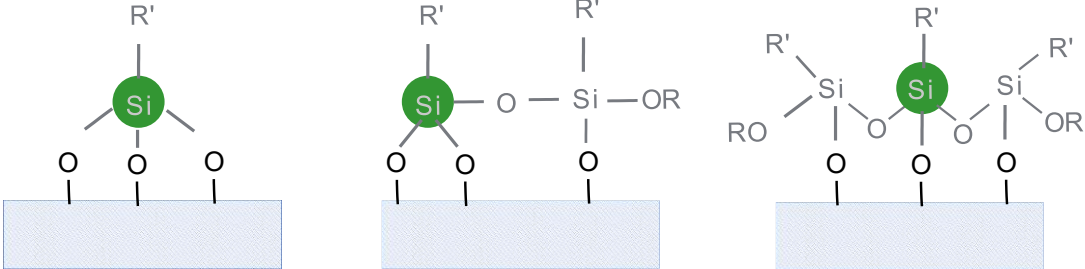
d. Wilhelm-Ostwald-Institut für Physikalische und Theoretische Chemie, Linnéstr. 2, 04103 Leipzig, Germany

Corresponding Authors

Jörg Matysik, Email: joerg.matysik@uni-leipzig.de

Section 1. Silicon species observable in ^{29}Si NMR spectra.

Table S1. Overview of the silicon species that are observed in ^{29}Si NMR with the respective chemical shifts. R is a hydrogen or methyl group, R' is the propyl chain with a thiol or sulfonic acid functionality.

| | | |
|---|---|---|
| <p>Q₂ / -93 ppm</p>  | <p>Q₃ / -103 ppm</p>  | <p>Q₄ / -113 ppm</p>  |
| <p>T₂ species / -59 ppm</p>  | | |
| <p>T₃ species / -68 ppm</p>  | | |

The observed silicon species are silicon oxides, the specific types are classified according to the number of siloxane bonds. Silicon with four oxygen bridges is referred to as quaternary (Q), while three oxygen bridges are referred to as a tertiary (T) species. The index represents the number of adjacent silicon atoms that are bound via a siloxane bond. R is a methyl group or a proton. A further distinction between the different structural motifs of the silicon species as shown in the rows of Table S1 was not achieved by NMR. R' is the propyl chain with a thiol or sulfonic acid functionality. A T₁ species was not observed.

Table S2. Summary of the deconvolution parameters of the ^{29}Si CPMAS NMR spectra.

| | Chemical shift [ppm] | Area [a.u.] | FWHM [Hz] |
|-----------------------------|----------------------|----------------|-----------|
| PMGB | | | |
| Q ₂ | - 93 | 30000 ± 10000 | 332 |
| Q ₃ | - 103 | 550000 ± 30000 | 477 |
| Q ₄ | - 113 | 590000 ± 50000 | 915 |
| PMGB-SH | | | |
| T ₂ | - 59 | 120000 ± 20000 | 506 |
| T ₃ | - 68 | 50000 ± 20000 | 463 |
| Q ₃ | - 103 | 310000 ± 10000 | 661 |
| Q ₄ | - 113 | 310000 ± 20000 | 663 |
| PMGB-SO₃H | | | |
| T ₂ | - 59 | 90000 ± 10000 | 613 |
| T ₃ | - 68 | 109000 ± 9000 | 510 |
| Q ₃ | - 102 | 210000 ± 10000 | 645 |
| Q ₄ | - 113 | 210000 ± 10000 | 722 |

Table S3. Summary of the deconvolution parameters of the ^{29}Si DPMAS NMR spectrum of the raw PMGB.

| | Chemical shift [ppm] | Area [a.u.] |
|----------------|----------------------|----------------|
| PMGB | | |
| Q ₂ | - 93 | 4000 ± 1000 |
| Q ₃ | - 103 | 70000 ± 7000 |
| Q ₄ | - 113 | 250000 ± 25000 |

The ratios between Q₂ and Q₃ species for raw PMGB are similar for CP and DP experiments. In both types of experiments, 5% of the species are assigned to Q₂, while 95% are Q₃.

Section 2. Characterization of PMGB, PMGB-SH and PMGB-SO₃H.

Table S4. Textural data from N₂ sorption.

| Sample | $A_{\text{BET}} / \text{m}^2 \text{g}^{-1}$ | $V_p / \text{cm}^3 \text{g}^{-1}$ | w_p / nm | $V_p / \text{cm}^3 \text{g}^{-1}$ (microporosity) |
|-----------------------------|---|-----------------------------------|-------------------|--|
| PMGB | 106 ± 3 | 0.21 ± 0.01 | 14.1 ± 0.4 | 0.00 |
| PMGB-SH | 70 ± 2 | 0.18 ± 0.01 | 12.8 ± 0.4 | 0.00 |
| PMGB-SO₃H | 84 ± 3 | 0.19 ± 0.01 | 13.8 ± 0.4 | 0.00 |

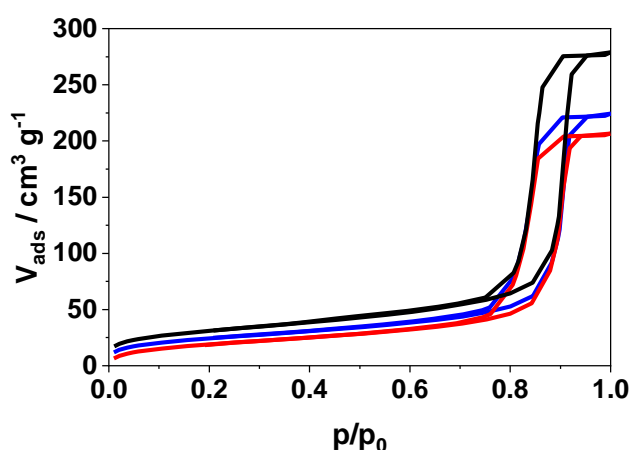


Figure S1. N₂ sorption isotherms of PMGB (black), PMGB-SH (red) and PMGB-SO₃H (blue).

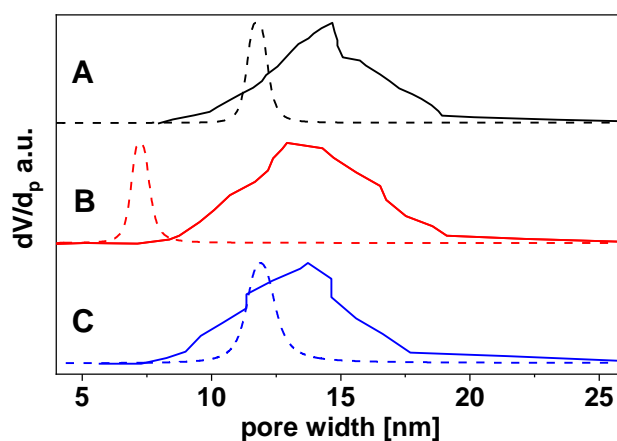


Figure S2. Pore width distributions from N₂ sorption (solid) and from HP ¹²⁹Xe NMR (dashed) of PMGB (black), PMGB-SH (red) and PMGB-SO₃H (blue).

Table S5. Carbon and Sulfur contents of the samples.

| Sample | Carbon content / wt.-% | Sulfur content / wt.-% |
|-----------------------------|------------------------|------------------------|
| PMGB | 0.14 ± 0.005 | 0.12 ± 0.01 |
| PMGB-SH | 2.29 ± 0.05 | 1.78 ± 0.09 |
| PMGB-SO₃H | 1.41 ± 0.05 | 1.03 ± 0.05 |

Section 3. Raman Spectra from Quantum Chemical Calculations.

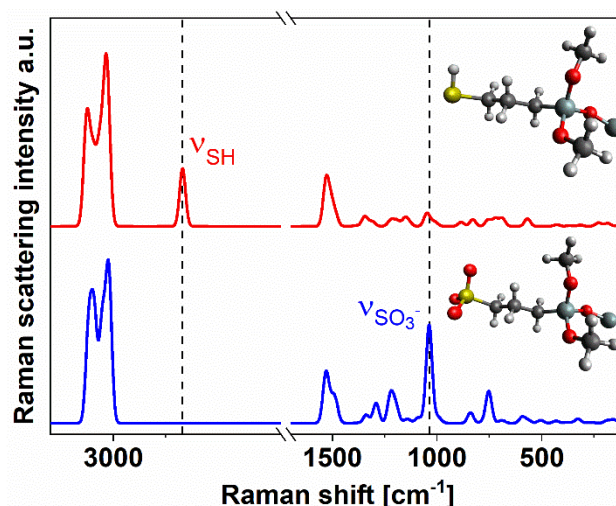


Figure S3. Simulated Raman spectra for PMGB-SH (red) and PMGB-SO₃⁻ (blue) models. The employed molecular structures are shown as insets with the following color coding: hydrogen (light gray), carbon (dark gray), oxygen (red), sulfur (yellow), and silicon (grey).

Starting structures for the molecular models of PMGB-SH and PMGB-SO₃⁻ were generated with TmoleX¹ and are shown as insets in Fig. S2. These structures were optimized using the B3LYP hybrid functional²⁻⁴ in combination with the 6-31G* basis set.⁵ For both molecules, all calculated vibrational frequencies were positive indicating that the optimized structures correspond to minima on the potential energy surfaces. Subsequently, Raman intensities were determined at the same level of theory. The quantum chemical calculations employed the Gaussian 16 software suite.⁶

These calculations reproduced the characteristic peaks found experimentally: For PMGB-SH, the S-H stretching vibration is located at 2670 cm⁻¹ and in case of PMGB-SO₃⁻, an additional peak at 1037 cm⁻¹ is obtained.

Section 4. Integral equivalents from ^{13}C CP-MAS NMR of PMGB-SH.

The experiments were performed with different CP contact times to evaluate quantitative integrals.

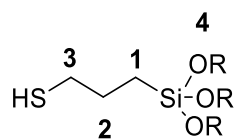


Figure S4. Structure of MPTMS. R can be either a residual methoxy group or a silicon species.

Table S6. Integral equivalents from ^{13}C CP-MAS NMR with different contact times.

| CP contact time | C1 14 ppm | Collapsed C2 and C3 at 30 ppm | C4 62 ppm |
|-----------------|--------------|----------------------------------|--------------|
| 1 ms | 1.15 | 1.85 | 0.52 |
| 4 ms | 1.02 | 1.98 | 0.38 |
| 8 ms | 1.02 | 1.98 | 0.41 |

References

- (1) Steffen, C.; Thomas, K.; Huniar, U.; Hellweg, A.; Rubner, O.; Schroer, A. TmoleX-A Graphical User Interface for TURBOMOLE. *J. Comput. Chem.* **2010**, *31* (16), 2967–2970. <https://doi.org/10.1002/jcc.21576>.
- (2) Becke, A. D. Density-Functional Exchange-Energy Approximation with Correct Asymptotic Behavior. *Phys. Rev. A* **1988**, *38* (6), 3098–3100. <https://doi.org/10.1103/PhysRevA.38.3098>.
- (3) Lee, C.; Yang, W.; Parr, R. G. Development of the Colle-Salvetti Correlation-Energy Formula into a Functional of the Electron Density. *Phys. Rev. B* **1988**, *37* (2), 785–789. <https://doi.org/10.1103/PhysRevB.37.785>.
- (4) Becke, A. D. Density-functional Thermochemistry. III. The Role of Exact Exchange. *J. Chem. Phys.* **1993**, *98* (7), 5648–5652. <https://doi.org/10.1063/1.464913>.
- (5) Hehre, W. J.; Ditchfield, R.; Pople, J. A. Self-Consistent Molecular Orbital Methods. XII. Further Extensions of Gaussian-Type Basis Sets for Use in Molecular Orbital Studies of Organic Molecules. *J. Chem. Phys.* **1972**, *56* (5), 2257–2261. <https://doi.org/10.1063/1.1677527>.
- (6) Frisch, M. J.; Trucks, G. W.; Schlegel, H. B.; Scuseria, G. E.; Robb, M. A.; Cheeseman, J. R.; Scalmani, G.; Barone, V.; Petersson, G. A.; Nakatsuji, H.; Li, X.; Caricato, M.; Marenich, A. V.; Bloino, J.; Janesko, B. G.; Gomperts, R.; Mennucci, B.; Hratchian, H. P.; Ortiz, J. V.; Izmaylov, A. F.; Sonnenberg, J. L.; Williams-Young, D.; Ding, F.; Lipparini, F.; Egidi, F.; Goings, J.; Peng, B.; Petrone, A.; Henderson, T.; Ranasinghe, D.; Zakrzewski, V. G.; Gao, J.; Rega, N.; Zheng, G.; Liang, W.; Hada, M.; Ehara, M.; Toyota, K.; Fukuda, R.; Hasegawa, J.; Ishida, M.; Nakajima, T.; Honda, Y.; Kitao, O.; Nakai, H.; Vreven, T.; Throssell, K.; Montgomery Jr., J. A.; Peralta, J. E.; Ogliaro, F.; Bearpark, M. J.; Heyd, J. J.; Brothers, E. N.; Kudin, K. N.; Staroverov, V. N.; Keith, T. A.; Kobayashi, R.; Normand, J.;

Raghavachari, K.; Rendell, A. P.; Burant, J. C.; Iyengar, S. S.; Tomasi, J.; Cossi, M.; Millam, J. M.; Klene, M.; Adamo, C.; Cammi, R.; Ochterski, J. W.; Martin, R. L.; Morokuma, K.; Farkas, O.; Foresman, J. B.; Fox, D. J. Gaussian 16 Revision C.01. 2016.